

Improving the Water Oxidation Efficiency with a Light-Induced Electric Field in Nanograting Photoanodes

Wenrong Wang,^{†,‡,§,¶} Beidou Guo,^{‡,§,¶} Haitao Dai,^{||} Chang Zhao,^{‡,§} Guancai Xie,^{‡,§} Renping Ma,[‡] Muhammad Zain Akram,^{‡,§} Hangyong Shan,[⊥] Congzhong Cai,[†] Zheyu Fang,^{*,⊥,||} and Jian Ru Gong^{*,‡,§,||}

[†]State Key Laboratory of Coal Mine Disaster Dynamics and Control, Department of Applied Physics, Chongqing University, Chongqing 400044, China

[‡]Chinese Academy of Sciences (CAS) Center for Excellence in Nanoscience, CAS Key Laboratory of Nanosystem and Hierarchy Fabrication, National Center for Nanoscience and Technology, Beijing 100190, China

[§]University of CAS, Beijing 100049, China

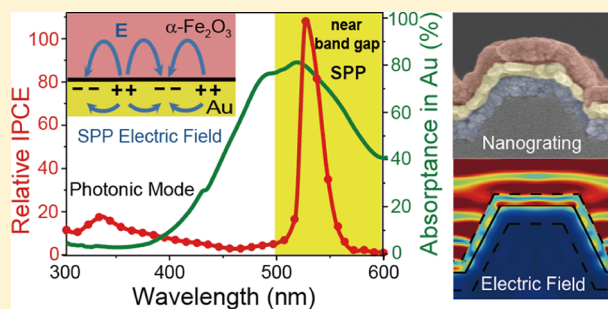
^{||}Tianjin Key Laboratory of Low Dimensional Materials Physics and Preparing Technology, School of Science, Tianjin University, Tianjin 300072, China

[⊥]School of Physics, State Key Lab for Mesoscopic Physics, Academy for Advanced Interdisciplinary Studies, Collaborative Innovation Center of Quantum Matter, and Nano-optoelectronics Frontier Center of Ministry of Education, Peking University, Beijing 100871, China

S Supporting Information

ABSTRACT: Severe charge recombination in solar water-splitting devices significantly limits their performance. To address this issue, we design a frustum of a cone nanograting configuration by taking the hematite and Au-based thin-film photoanode as a model system, which greatly improves the photoelectrochemical water oxidation activity, affording an approximately 10-fold increase in the photocurrent density at 1.23 V versus the reversible hydrogen electrode compared to the planar counterpart. The surface plasmon polariton-induced electric field in hematite plays a dominant role in efficiency enhancement by facilitating charge separation, thus dramatically increasing the incident photon-to-current efficiency (IPCE) by more than 2 orders of magnitude in the near band gap of hematite. And the relatively weak electric field caused by light scattering in the nanograting structure is responsible for the approximate maximum 20-fold increase in IPCE within a broadband wavelength range. Our scalable strategy can be generalized to other solar energy conversion systems.

KEYWORDS: Surface plasmon polaritons, electric field, nanograting, solar water splitting, charge separation, light scattering



Solar water splitting over semiconductors is a promising way to convert sunlight into renewable hydrogen energy.^{1–8} However, mainly because of the severe recombination of photogenerated charge carriers,^{9,10} current practical efficiencies are far from the ideal theoretical values.¹¹ Introducing built-in electric fields by various junctions, owing to the difference in the individual Fermi levels, has been a commonly adopted strategy for charge separation.^{12–14} The electric field, which enables the separation of electrons and holes immediately after their generation, is a good candidate for charge separation tuning.¹⁵ Nevertheless, the electric field is distributed only in the small region at the junction interface. Otherwise, junctions suffer from interface issues, such as abrupt composition changes and large lattice mismatches, which are detrimental to charger transfer across interfaces. Recently, polarization electric fields with the ability to promote charge separation both in the bulk and on the surface of

semiconductors have shown great potential in photocatalysis.¹⁶ For example, the sawtoothlike potential distribution in the zincblende/wurtzite superlattice, which has the same composition, good lattice match, and type II band alignment, facilitates charge separation in the bulk material.¹⁷ Unfortunately, precise control of the electric field distribution by facile modulation of the material microstructure is still difficult now. In addition, more effective external polarization methods need to be developed. To overcome the problems mentioned above, a new strategy for controlling the built-in electric field of materials for charge separation is urgently needed to improve the water-splitting performance.

Received: May 24, 2019

Revised: August 9, 2019

Published: August 20, 2019

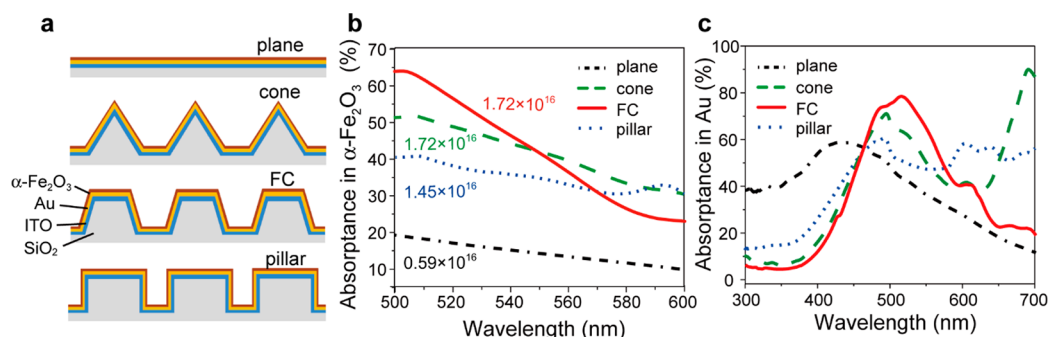


Figure 1. Geometry and light absorption of nanogratings. (a) Schematic geometries, FDTD-simulated absorption curves with the labeled total absorbed photon numbers of (b) α -Fe₂O₃ and (c) Au for the cone, FC, and pillar nanograting and plane structures of SiO₂/ITO/Au/ α -Fe₂O₃.

Induced by an electromagnetic wave (light), surface plasmon resonance (SPR), which is the collective and coherent oscillation of conduction electrons of a metal at a resonance frequency relative to the lattice of positive ions, can form an alternating electric field.¹⁸ The electric field caused by SPR has a few advantages for solar water splitting. First, the strong field associated with the SPR is evanescent into dielectric materials of up to approximately half the involved wavelength,¹⁹ which is larger than the charge collection distance (charge diffusion length + width of space charge region) in most semiconductors (e.g., ~10 nm for hematite, α -Fe₂O₃),²⁰ possibly leading to more effective separation of photogenerated charges. Second, the SPR electric field can be created in the single material to facilitate the charge separation, bypassing the common problems of interfacial charge recombination due to great disparities in the composition and lattice constant or band misalignment between different materials.²¹ Third, the SPR electric field can be easily modulated by changing irradiation parameters besides the geometries of materials.^{22–24} SPR can be classified into two distinct forms: localized surface plasmon resonance (LSPR) and surface plasmon polaritons (SPP).^{25,26} Both have been used to improve the solar water-splitting performance^{27–29} when embedding gold (Au) nanoparticles into a thin α -Fe₂O₃ film,³⁰ incorporating α -Fe₂O₃ nanorods into a plasmonic Au nanohole array pattern,²⁶ or fabricating Au nanopillars with an α -Fe₂O₃ coating.³¹ Au is commonly used as a plasmonic metal owing to the tunable plasmon resonances at ultraviolet and visible frequencies, relatively large optical cross sections, and thermodynamic or kinetic stability under harsh conditions (pH and potential) for water splitting.³² Except for the beneficial built-in electric field at the metal/semiconductor heterojunction mentioned above,³³ there are three main mechanisms for efficiency enhancement, all of which are due to an increase in light absorption: (1) plasmon resonance energy transfer (PRET), which might arise when light absorption of metals and semiconductors overlaps;³⁴ (2) hot electron transfer, occurring at energies well below the semiconductor band gap;^{26,34,35} and (3) scattering, which can happen over a broad spectral region.²¹ And PRET or hot electron production usually occurs at small particle sizes (<100 nm), and scattering becomes more probable at large particle sizes.³² Also, hot electron injection mainly occurs in the near-infrared (NIR).^{36,37} Linic et al. have reported²⁸ that the SPR-induced electric field distributed close to the semiconductor is conducive to charge separation in the near-surface region of the semiconductor and can promote photocatalytic performance. Little work, however, has been carried out to explore the effect of the SPR-induced electric field on charge separation in

semiconductors. Compared to the extremely confined LSPR, the evanescent field induced by SPP has a much longer decay length in the direction normal to the metal/semiconductor interface^{38–40} and also propagates along the metal/dielectric interface,^{22,41} both of which lead to a larger distribution of the electric field in the semiconductor for potentially more efficient charge separation.^{26,35,42–44} In addition, in patterned nanostructures, photonic light scattering also can induce an electric field. In contrast to the SPR mode, which has the largest field amplitude at the metal/semiconductor interface, the electric field of the light scattering is maximized in the middle of the semiconductor layer over a much broader spectral region.^{29,31} Although the electric field of light scattering is relatively weak compared to SPR, this electric field caused by the polarization of oscillating light will play a role in hindering the charge recombination.

In this report, we design the α -Fe₂O₃ and Au-based thin-film photoanode with a frustum of a cone (FC) nanograting structure, which greatly improves the photoelectrochemical (PEC) oxygen evolution reaction (OER) with an ~10-fold increase in the photocurrent density at 1.23 V versus the reversible hydrogen electrode (V_{RHE}) compared to the planar counterpart. α -Fe₂O₃ is chosen as a semiconductor model because of its stable, nontoxic, low-cost, earth-abundant properties, and a suitable band structure for water oxidation: the bottleneck of water splitting.^{20,21,43,45} Half of the maximum possible photocurrent density lies in the near band gap of α -Fe₂O₃ (500–600 nm),^{46,47} but its poor absorption coefficient at the near band gap seriously limits the α -Fe₂O₃ performance.⁴⁸ To improve the PEC OER more effectively, we choose the SPP resonance peak at the near band gap of α -Fe₂O₃. The SPP-induced electric field in α -Fe₂O₃ plays a dominant role in efficiency enhancement by facilitating charge separation, thus dramatically increasing the incident photon-to-current efficiency (IPCE) by more than 2 orders of magnitude at the near band gap of α -Fe₂O₃, and the relatively weak electric field caused by light scattering in the nanograting structure is responsible for the approximate maximum 20-fold increase in IPCE within a broadband wavelength range. This scalable strategy provides insightful guidance to various solar energy conversion systems.

The wavelength-dependent SPP can be obtained by tuning the geometry and periodicity of the grating and the dielectric property of materials.^{34,40,41} Using polystyrene (PS) microspheres as a mask for reactive ion etching (RIE) is an effective and low-cost method of preparing a well-defined nanograting structure over a large area. Using this method, three kinds of typical nanograting geometries (i.e., cone, FC, and pillar) can

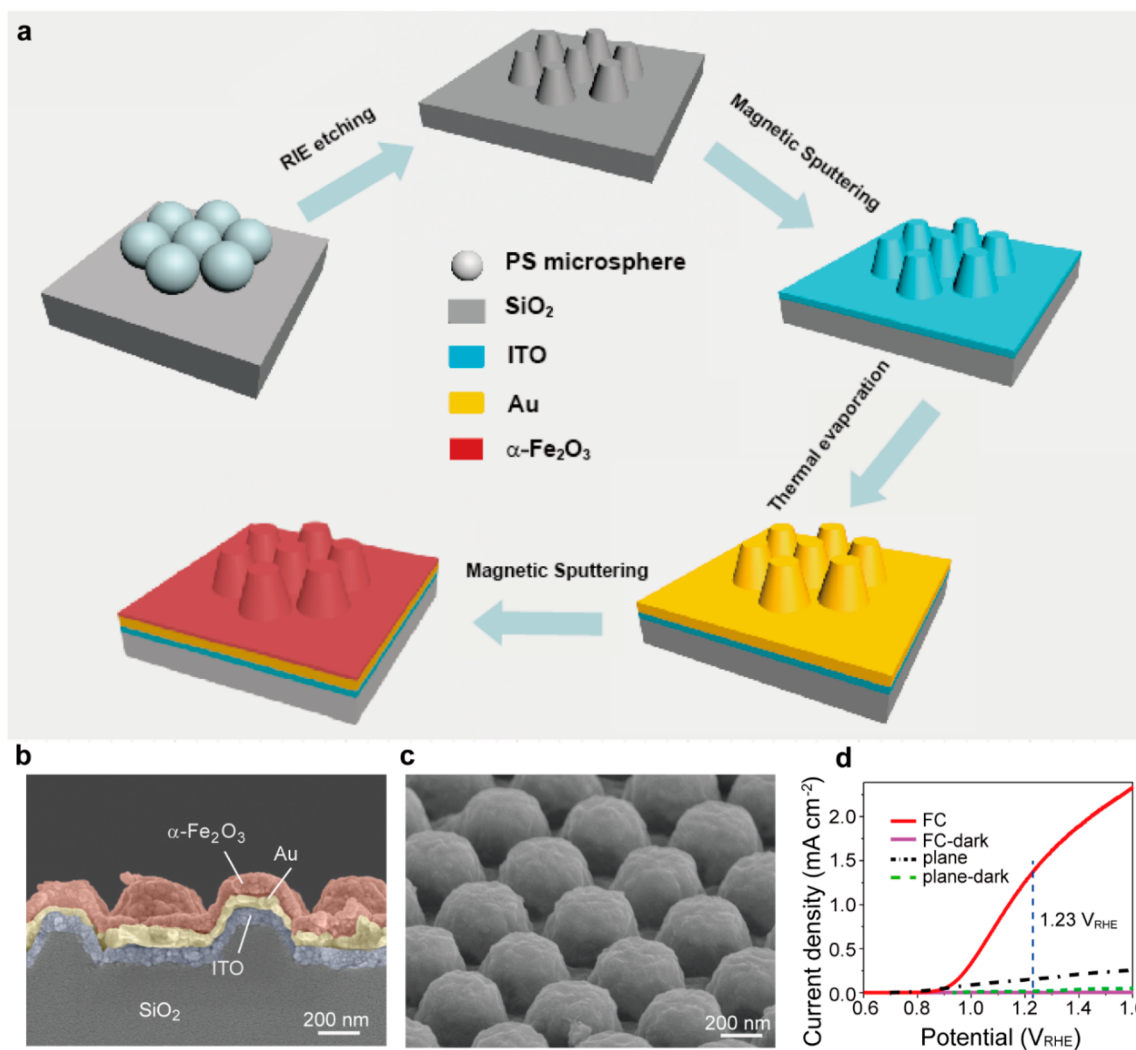


Figure 2. Schematic of the fabrication process, structure, and OER activity of the SiO₂/ITO/Au/α-Fe₂O₃ anodes. (a) Schematic of the fabrication process for the FC nanograting of SiO₂/ITO/Au/α-Fe₂O₃. (b) Cross-sectional and (c) tilted SEM images of the SiO₂/ITO/Au/α-Fe₂O₃ anode with the FC nanograting structure (pitch = 600 nm, height = 300 nm, base diameter = 440 nm, and top diameter = 200 nm). (d) Photocurrent and dark current densities of the SiO₂/ITO/Au/α-Fe₂O₃ photoanodes with the FC nanograting and planar geometries.

be constructed.⁴⁹ Here, we have investigated these three typical nanograting geometries with the same height and increasing angles between the side wall and the horizontal plane as well as the planar geometry, aiming to select the optimal structure for creating the strongest SPP resonance at the near band gap of α-Fe₂O₃ (Figure 1a).^{49,50} It is known that the collective charge oscillation of SPP at a metal surface usually gives rise to peaks in the spectrally resolved absorption of the metal.^{29,51} Therefore, the SPP resonance peak can be inferred by the absorption peak of the metal. However, because of the complex light–matter interaction between the semiconductor (α-Fe₂O₃) and metal (Au) caused by material and geometric properties in this system, light absorption in α-Fe₂O₃ and Au cannot be experimentally distinguished. We have therefore used finite-difference-time-domain (FDTD) simulations,^{52,53} a 3D/2D Maxwell solver for nanophotonic devices, to elucidate the light absorption of α-Fe₂O₃ and Au in all of the samples. In addition, the simulation has the advantage of saving time and cost for trial-and-error experiments.⁵⁴ As shown in Figure 1b,c, the FC grating obtains the maximum light absorbance in the range of 500–600 nm for both α-

Fe₂O₃ and Au among all geometries, making it a perfect geometry for studying the SPP effect in α-Fe₂O₃.

The process for fabricating the FC nanograting of the SiO₂/ITO/Au/α-Fe₂O₃ photoanode is shown in Figure 2a. Briefly, a SiO₂ substrate was first covered with a monolayer mask, which is composed of a six-party close-packed PS microspheres⁵⁰ (Figure S1). Next, RIE was employed to prepare a SiO₂ FC nanograting with long-range order (Figure S2a). After magnetically sputtering an ITO adhesion layer⁵⁵ onto the SiO₂ FC nanograting (Figure S2b), Au was thermally evaporated off of the top (Figure S2c). The ITO film has little effect on light absorption because light cannot penetrate the uniform, dense 100-nm-thick Au film. After that, a homogeneous Fe layer was magnetically sputtered as the top layer. Finally, the SiO₂/ITO/Au/α-Fe₂O₃ photoanode with the FC nanograting structure was obtained after annealing the assembled structure at high temperature in air (Figure S2d). The cross-sectional scanning electron microscopy (SEM) image of this photoanode (Figure 2b) clearly shows a high-quality conformal coating of α-Fe₂O₃ (~50 nm), Au (~100 nm), and ITO (~150 nm) on the SiO₂ substrate, indicating that the well-defined SiO₂/ITO/Au/α-Fe₂O₃ FC nanograting

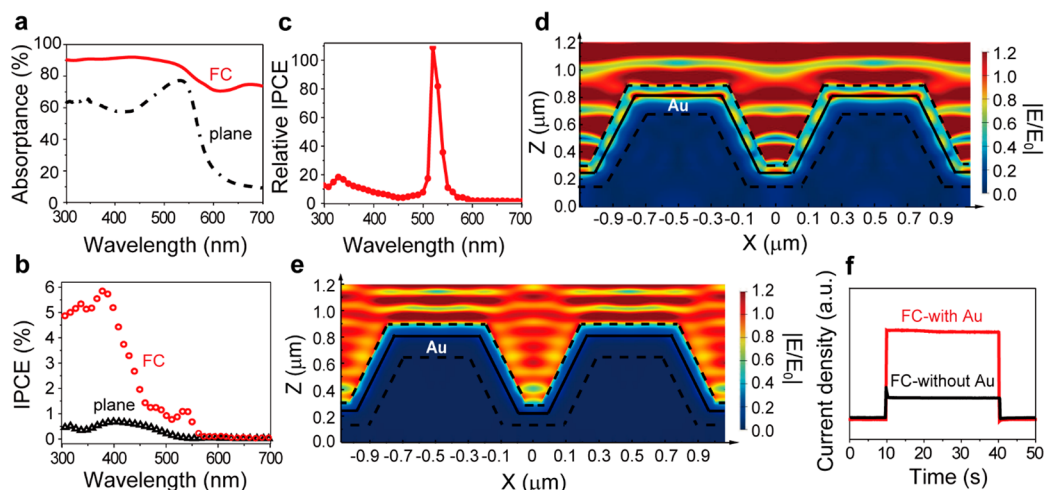


Figure 3. Mechanistic investigations of improvement in the OER activity. (a) Experimental absorption spectra and (b) spectrally resolved IPCE curves of the FC nanograting and planar structures of $\text{SiO}_2/\text{ITO}/\text{Au}/\alpha\text{-Fe}_2\text{O}_3$ in the wavelength range of 300–700 nm at $1.23 V_{\text{RHE}}$. (c) Relative IPCE curve of the $\text{SiO}_2/\text{ITO}/\text{Au}/\alpha\text{-Fe}_2\text{O}_3$ photoanode with the FC nanograting structure, calculated by dividing its IPCE by that of the planar sample. (d) FDTD-simulated electric field $|E/E_0|$ distribution of FC nanograting structures of $\text{SiO}_2/\text{ITO}/\text{Au}/\alpha\text{-Fe}_2\text{O}_3$ at a wavelength of 516 nm. (e) FDTD simulated electric field $|E/E_0|$ distribution of the FC nanograting at a wavelength of 331 nm. (f) Transient photocurrents of the anodes with the FC nanograting with and without Au shown by light chopping current densities (light on/light off) as a function of time under irradiation at an applied potential of $1.23 V_{\text{RHE}}$.

structure was obtained. Tilted (Figure 2c) and top-view (Figure S3) SEM images show the high periodicity of the well-arranged FC nanograting, and X-ray diffraction confirms the formation of $\alpha\text{-Fe}_2\text{O}_3$ and Au in the sample (Figure S4). Compared to other reported Au nanoarray structures,^{29,31} our design economizes the amount of Au by coating a thin film with a smaller volume ratio in the electrode structure.

The PEC OER of the prepared photoanodes was evaluated in 1 M NaOH electrolyte (pH 13.6) without any sacrificial reagents using a three-electrode electrochemical system under 150 W xenon lamp irradiation with a light intensity of $\sim 450 \text{ mW cm}^{-2}$ (details in the Supporting Information). After the height, thickness, and pitch of the FC nanograting are optimized (Figures S5–S7), the $\text{SiO}_2/\text{ITO}/\text{Au}/\alpha\text{-Fe}_2\text{O}_3$ photoanode affords a photocurrent density of 1.33 mA cm^{-2} at $1.23 V_{\text{RHE}}$, which is ~ 10 times higher than that of the planar sample (0.15 mA cm^{-2}) under the same experimental conditions (Figure 2d). The photoanodes exhibit negligible dark current densities (less than 0.05 mA cm^{-2}) within the tested potential range, implying that the observed current densities under irradiation are related exclusively to photo-generated charge carriers.⁵⁶

To explore the underlying mechanism for the greatly improved OER activity of the photoanode with the FC nanograting structure, the light absorption property was first investigated with ultraviolet–visible (UV–vis) absorption spectra. The anode with the FC nanograting structure with $\sim 70\text{--}90\%$ light absorbance within the range of 300–700 nm shows a broadband absorption enhancement when compared to its planar counterpart with 10–80% light absorbance (Figure 3a). Similarly, an absorption increase in both experimental and simulated data is observed for the FC nanograting without $\alpha\text{-Fe}_2\text{O}_3$ and without Au compared to their planar counterparts, respectively (Figure S8). Therefore, the absorption enhancement is associated with the unique FC geometry. We also found that the absorption is most obviously enhanced in the long-wavelength range (500–700 nm) (Figure 3a), and the maximum enhancement is up to ~ 7 -fold. For the

samples without $\alpha\text{-Fe}_2\text{O}_3$ ($\text{SiO}_2/\text{ITO}/\text{Au}$), the absorption of the FC nanograting also has a significant enhancement (the maximum enhancement is up to ~ 6 -fold) in the long-wavelength range (500–700 nm) compared to the planar counterpart (Figure S8a,b), which is consistent with the absorption of the $\text{SiO}_2/\text{ITO}/\text{Au}/\alpha\text{-Fe}_2\text{O}_3$ samples (Figure 3a). However, there is no such significant absorption enhancement in the samples without Au ($\text{SiO}_2/\text{ITO}/\alpha\text{-Fe}_2\text{O}_3$) (Figure S8c,d), which indicates that the absorption enhancement is associated with Au. The above results indicate that the absorption enhancement in the photoanode is ascribed to the influence of the unique Au FC geometry.

The IPCE measurement was carried out to further investigate the anode activity at different wavelengths (Figure 3b). The anode with the FC nanograting geometry shows a substantially enhanced IPCE in a broadband wavelength range from 300 to 600 nm, when compared to the planar structure. The relative IPCE spectrum was obtained by dividing the IPCE of the anode with FC geometry by that of the planar sample (Figure 3c). A dramatic ~ 110 -fold IPCE increase at 516 nm is observed, over 2 orders of magnitude, which correlates well with the distinct SPP absorption peak of Au at 516 nm extracted by FDTD (Figure 1c), confirming that the increase in IPCE at 516 nm is mainly caused by the SPP of Au. In contrast, the SPP peak of Au in the disordered FC structure is weak and blue-shifted (Figure S9), indicating that the ordered grating can achieve a stronger SPP enhancement at the near band gap of $\alpha\text{-Fe}_2\text{O}_3$ compared to the disordered counterpart. As shown in Table S1, our relative IPCE value is $\sim 6\text{--}55$ times higher than those of the representative works based on the Au plasmon photoanodes.

Because of plasmon resonance, SPP of Au can create an electric field in $\alpha\text{-Fe}_2\text{O}_3$.²⁵ The distribution of the electric field in the FC nanograting structure at 516 nm was simulated by FDTD. The red and yellow colored areas display the strong electric field intensity in $\alpha\text{-Fe}_2\text{O}_3$ near the Au/ $\alpha\text{-Fe}_2\text{O}_3$ interface of the FC nanograting (yellow area, Figure 3d), and the electric field shows periodic fluctuation at the platform

Table 1. Tabular Summary of the Photocurrent Density, Absorbed Photon Number for α -Fe₂O₃, and Electric Field Intensity of the FC Nanograting with Different Heights and α -Fe₂O₃ Thicknesses

	FC (nm)	Photocurrent density (mA cm ⁻²) ^a	Photon number ^b	E/E ₀ ^c at 516 nm	E/E ₀ ^c at 331 nm
Height	300	1.33	4.79×10 ¹⁶	2.08	0.75
	400	1.15	3.87×10 ¹⁶	1.75	0.69
	500	0.77	4.95×10 ¹⁶	1.73	0.66
Thickness	50	1.33	4.79×10 ¹⁶	2.08	0.75
	100	1.21	6.13×10 ¹⁶	1.57	0.68
	130	0.50	5.04×10 ¹⁶	1.31	0.68

and side walls of the FC nanograting structure, which both propagates at the Au/ α -Fe₂O₃ interface and decays along the direction normal to the interface.^{38,40} It further confirms the presence of SPP with a resonance peak at 516 nm and also indicates that the SPP-induced electric field might contribute to the activity enhancement.

Furthermore, we investigated the influence of geometry parameters of the FC nanograting on the photoanode properties to understand the essence of the OER enhancement by SPP.^{25,27–29} First, the changes in the photocurrent, light absorption, and FDTD-simulated electric field intensity of the SiO₂/ITO/Au/ α -Fe₂O₃ anode with varying FC nanograting heights (300, 400, and 500 nm) were studied (Figure S5). The photocurrent density of SiO₂/ITO/Au/ α -Fe₂O₃ decreases with increasing height. In contrast, light absorption increases with increasing height, implying that light absorption is not the main reason for the photocurrent decrease. The electric field intensity in α -Fe₂O₃ near the Au/ α -Fe₂O₃ interface decreases with increasing height, which is in accordance with the experimentally observed changing trend in photocurrent density, indicating that the SPP-induced electric field intensity is closely related to the OER activity (Table 1). Next, we analyzed the influence of the α -Fe₂O₃ layer thickness (50, 100, and 130 nm) on the photoanode properties because the SPP effect also depends on the dielectric environment surrounding the metal.⁵⁷ Similar to the effect of height, both the photocurrent density and the electric field intensity decrease with increasing α -Fe₂O₃ thickness, while the changing trend in absorption is inconsistent with that of the photocurrent density (Figure S6, Table 1). Again, it corroborates the electric field intensity-dependent OER activity.

In addition to the SPP effect at the near band gap of α -Fe₂O₃ mentioned above, our photoelectrode with a nonplanar Au back contact has photonic light scattering,^{50,58} which can induce an electric field in the middle of the α -Fe₂O₃ layer in a much broader spectral region.^{25,31} In contrast to the SPP mode, which has the largest electric field at the resonant wavelength of 516 nm at the Au/ α -Fe₂O₃ interface, the photonic mode can be identified by the electric field at the nonresonant wavelength of 331 nm (far from the SPP resonance wavelength) in the α -Fe₂O₃ layer calculated by FDTD simulation,^{45,59} as for the approximate maximum 20-fold enhancement in IPCE over a broad spectral range (300–600 nm) (Figure 3b), whereas the evanescent field at the Au/ α -Fe₂O₃ interface is absent (Figure 3e). The electric field intensity in α -Fe₂O₃ at 331 nm (about one-third of that of SPP) decreases with increasing height and thickness the same

as the change in the geometry parameter for the SPP investigation, which is also in accordance with the observed changing trend in the photocurrent density. It further indicates that the electric field intensity caused by the photonic mode is closely related to the OER activity (Table 1).

We then looked into the charge separation behavior by measuring the transient photocurrent so as to further understand the reason for the OER activity enhancement (Figure 3f).^{56,60,61} The transient photocurrent of the FC nanograting without Au shows a spike upon sudden irradiation due to capacitive charging at the α -Fe₂O₃–electrolyte interface, which is due to recombination of the charge carriers. However, the spike disappears in the transient photocurrent of the FC nanograting with Au, displaying the beneficial role of Au in facilitating charge separation. After the introduction of Au, the energy barrier height at the Au and α -Fe₂O₃ Schottky junction hinders the transfer of photogenerated electrons from α -Fe₂O₃ to the substrate, and the formation of trap states at the interface causes charge recombination and Fermi-level pinning, which will limit the OER activity (Figure 4).⁶² However, the photocurrent increases (Figure S10), which confirms that the plasmonic effect of Au is dominant in this case because the light absorption of Au overlaps with that of α -Fe₂O₃ and light energy transfers from Au to α -Fe₂O₃ by PRET. The light absorption increase owing to PRET is usually taken as the

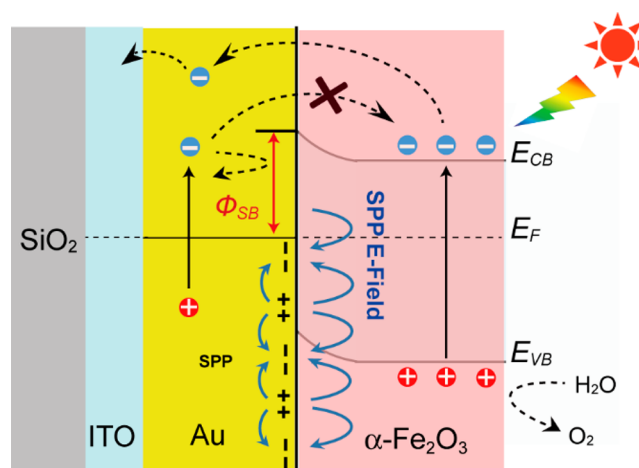


Figure 4. Energy-level diagram and SPP-induced electric field distribution of the SiO₂/ITO/Au/ α -Fe₂O₃ FC nanograting structure (E_{CB} , conduction band; E_{VB} , valence band; E_F , Fermi level; Φ_{SB} , Schottky barrier).

reason for the activity enhancement,³² but it is inconsistent with the relation between light absorption and photocurrent in our case (Table 1). In addition, the photocurrent spike is not caused by any modification of the electrode surface because there is little change in the α -Fe₂O₃ surface structure. Other possible factors which might affect the OER activity are also considered. First, the role of Au catalysis in the electrolyte is considered because it often exists in Au particles to lower the overpotential of the photoelectrochemical reactions.^{32,62} However, the onset potential of the FC photoanode (Figure 2d) seems the same as that of the planar electrode, which means that the overpotential in the photoelectrochemical reactions does not change, assuming that the photovoltages of both electrodes are the same because they are composed of the same materials with the same Fermi-level difference. Therefore, the Au film underneath the dense α -Fe₂O₃ layer does not participate in the surface water oxidation reaction, and the role of Au catalysis can be excluded. Second, the hot electron transfer is most probable at energies well below the semiconductor band gap for small particle sizes (<100 nm),³² which is not our case (Figure 4).³⁴ Third, the large specific surface area of the nanograting structure is also a factor which might affect the OER activity. The SiO₂/ITO/ α -Fe₂O₃ (without Au) FC nanograting structure has the same specific surface area as the SiO₂/ITO/Au/ α -Fe₂O₃ FC nanograting structure. However, the photocurrent densities of the SiO₂/ITO/ α -Fe₂O₃ (without Au) FC nanograting structure (0.15 mA cm⁻² at 1.23 V_{RHE}) are about 10 times lower than that of the SiO₂/ITO/Au/ α -Fe₂O₃ FC nanograting structure (1.33 mA cm⁻² at 1.23 V_{RHE}) (Figure S10), which indicates that the PEC performance improvement does not come from the large specific surface area in our case. Taken together, the above analysis indicates that the SPP-induced electric field in α -Fe₂O₃ not only promotes the charge separation within α -Fe₂O₃ but also causes the change of the electric field distribution on the α -Fe₂O₃ surface. It retards the charge recombination and makes the photocurrent spike disappear, which is in line with the relation between the electric field intensity and the photocurrent (Table 1). Therefore, it can be inferred that the electric field induced by SPP plays a dominant role in the enhancement of the OER activity at the near band gap of hematite with the FC nanograting geometry (Figure 4), and the relatively weak electric field in α -Fe₂O₃ determined by light scattering is also favorable for hindering charge separation, thus improving the OER efficiency.

In summary, the well-defined periodic FC nanograting of the SiO₂/ITO/Au/ α -Fe₂O₃ photoanode was successfully fabricated at low cost and afforded a greatly improved PEC OER activity. The surface plasmon polariton-induced electric field in hematite plays a dominant role in efficiency enhancement by facilitating charge separation, thus dramatically increasing the IPCE by more than 2 orders of magnitude at the near band gap of hematite, and the weak electric field caused by the photonic mode in the nanograting structure is responsible for the approximately maximum 20-fold increase in IPCE within a broadband wavelength range. Our results prove the charge-separation effect of the light-induced electric field in the semiconductor photoabsorber by the judicious design of the device geometry, and this scaling strategy is promising for other solar energy conversion systems.

■ ASSOCIATED CONTENT

Supporting Information

The Supporting Information is available free of charge on the ACS Publications website at DOI: 10.1021/acs.nanolett.9b02122.

Experimental details, SEM images of a monolayer of PS microspheres and NFC arrays, data and analysis for the optimization of the height and pitch of the NFC arrays, and the α -Fe₂O₃ film thickness (PDF)

■ AUTHOR INFORMATION

Corresponding Authors

*E-mail: zhyfang@pku.edu.cn.

*E-mail: gongjr@nanoctr.cn.

ORCID

Hangyong Shan: 0000-0003-3988-4870

Zheyu Fang: 0000-0001-5780-0728

Jian Ru Gong: 0000-0003-1512-4762

Author Contributions

#These authors contributed equally.

Notes

The authors declare no competing financial interest.

■ ACKNOWLEDGMENTS

The authors acknowledge financial support from the National Natural Science Foundation of China (21422303, 11604062, 11674012, 61521004, and 21790364), National Key R&D Program “nanotechnology” special focus (2016YFA0201600 and 2015CB932403), the Graduate Scientific Research and Innovation Foundation of Chongqing (CXB243), the Beijing Natural Science Foundation (2142036 and Z180011), and the Knowledge Innovation Program and Youth Innovation Promotion Association of CAS, National Program for Support of Top-Notch Young Professionals (W02070003)

■ REFERENCES

- (1) Walter, M. G.; Warren, E. L.; McKone, J. R.; Boettcher, S. W.; Mi, Q.; Santori, E. A.; Lewis, N. S. *Chem. Rev.* **2010**, *110* (11), 6446–6473.
- (2) Grätzel, M. *Nature* **2001**, *414* (6861), 338–344.
- (3) van de Krol, R.; Liang, Y.; Schoonman, J. J. *Mater. Chem.* **2008**, *18* (20), 2311–2320.
- (4) Tachibana, Y.; Vayssieres, L.; Durrant, J. R. *Nat. Photonics* **2012**, *6* (8), 511–518.
- (5) Fujishima, A.; Honda, K. *Nature* **1972**, *238* (5358), 37–38.
- (6) Lewis, N. S.; Nocera, D. G. *Proc. Natl. Acad. Sci. U. S. A.* **2006**, *103* (43), 15729–15735.
- (7) Li, Z.; Luo, W.; Zhang, M.; Feng, J.; Zou, Z. *Energy Environ. Sci.* **2013**, *6* (2), 347–370.
- (8) Guo, B.; Batoool, A.; Xie, G.; Boddula, R.; Tian, L.; Jan, S. U.; Gong, J. R. *Nano Lett.* **2018**, *18* (2), 1516–1521.
- (9) Kesselman, J. M.; Shreve, G. A.; Hoffmann, M. R.; Lewis, N. S. *J. Phys. Chem.* **1994**, *98*, 13385–13395.
- (10) Dotan, H.; Sivula, K.; Grätzel, M.; Rothschild, A.; Warren, S. C. *Energy Environ. Sci.* **2011**, *4* (3), 958–964.
- (11) Bolton, J. R.; Stricklert, S. J.; Connolly, J. *Nature* **1985**, *316*, 495–500.
- (12) Mayer, M. T.; Lin, Y.; Yuan, G.; Wang, D. *Acc. Chem. Res.* **2013**, *46* (7), 1558–66.
- (13) Li, H.; Zhou, Y.; Tu, W.; Ye, J.; Zou, Z. *Adv. Funct. Mater.* **2015**, *25* (7), 998–1013.

- (14) Xie, G.; Guan, L.; Zhang, L.; Guo, B.; Batool, A.; Xin, Q.; Boddula, R.; Jan, S. U.; Gong, J. R. *Nano Lett.* **2019**, *19* (2), 1234–1241.
- (15) Li, J.; Cai, L.; Shang, J.; Yu, Y.; Zhang, L. *Adv. Mater.* **2016**, *28* (21), 4059–64.
- (16) Chen, F.; Huang, H.; Guo, L.; Zhang, Y.; Ma, T. *Angew. Chem., Int. Ed.* **2019**, *58*, 10061.
- (17) Zhang, K.; Dai, Y.; Zhou, Z.; Ullah Jan, S.; Guo, L.; Gong, J. R. *Nano Energy* **2017**, *41*, 101–108.
- (18) Lu, X.; Rycenga, M.; Skrabalak, S. E.; Wiley, B.; Xia, Y. *Annu. Rev. Phys. Chem.* **2009**, *60*, 167–92.
- (19) Tvingstedt, K.; Persson, N.-K.; Inganäs, O. *Appl. Phys. Lett.* **2007**, *91* (11), 113514–113516.
- (20) Zhang, K.; Dong, T.; Xie, G.; Guan, L.; Guo, B.; Xiang, Q.; Dai, Y.; Tian, L.; Batool, A.; Jan, S. U.; Boddula, R.; Thebo, A. A.; Gong, J. R. *ACS Appl. Mater. Interfaces* **2017**, *9* (49), 42723–42733.
- (21) Wu, N. *Nanoscale* **2018**, *10* (6), 2679–2696.
- (22) Sambles, J. R.; Bradbery, G. W.; Yang, F. *Contemp. Phys.* **1991**, *32* (3), 173–183.
- (23) Dionne, J. A.; Sweatlock, L. A.; Atwater, H. A.; Polman, A. *Phys. Rev. B: Condens. Matter Mater. Phys.* **2005**, *72* (7), No. 075405.
- (24) Dolev, I.; Volodarsky, M.; Porat, G.; Arie, A. *Opt. Lett.* **2011**, *36* (9), 1584–1586.
- (25) Atwater, H. A.; Polman, A. *Nat. Mater.* **2010**, *9* (3), 205–213.
- (26) Li, J.; Cushing, S. K.; Zheng, P.; Meng, F.; Chu, D.; Wu, N. *Nat. Commun.* **2013**, *4*, 2651–2658.
- (27) Sheldon, M. T.; Groep, J. v. d.; Brown, A. M.; Polman, A.; Atwater, H. A. *Science* **2014**, *346* (6211), 828–831.
- (28) Ingram, D. B.; Linic, S. *J. Am. Chem. Soc.* **2011**, *133* (14), 5202–5205.
- (29) Xu, R.; Wen, L.; Wang, Z.; Zhao, H.; Xu, S.; Mi, Y.; Xu, Y.; Sommerfeld, M.; Fang, Y.; Lei, Y. *ACS Nano* **2017**, *11* (7), 7382–7389.
- (30) Archana, P. S.; Pachauri, N.; Shan, Z. C.; Pan, S. L.; Gupta, A. J. *J. Phys. Chem. C* **2015**, *119* (27), 15506–15516.
- (31) Gao, H.; Liu, C.; Jeong, H. E.; Yang, P. *ACS Nano* **2012**, *6* (1), 234–240.
- (32) Warren, S. C.; Thimsen, E. *Energy Environ. Sci.* **2012**, *5* (1), 5133–5146.
- (33) Mubeen, S.; Singh, N.; Lee, J.; Stucky, G. D.; Moskovits, M.; McFarland, E. W. *Nano Lett.* **2013**, *13* (5), 2110–5.
- (34) Cushing, S. K.; Wu, N. *Electrochem. Soc. Interface* **2013**, *22* (2), 63–67.
- (35) Zheng, Z.; Xie, W.; Huang, B.; Dai, Y. *Chem. - Eur. J.* **2018**, *24* (69), 18322–18333.
- (36) Cushing, S. K.; Bristow, A. D.; Wu, N. *Phys. Chem. Chem. Phys.* **2015**, *17* (44), 30013–22.
- (37) Sobhani, A.; Knight, M. W.; Wang, Y.; Zheng, B.; King, N. S.; Brown, L. V.; Fang, Z.; Nordlander, P.; Halas, N. *Nat. Commun.* **2013**, *4*, 1643.
- (38) Schuller, J. A.; Barnard, E. S.; Cai, W.; Jun, Y. C.; White, J. S.; Brongersma, M. L. *Nat. Mater.* **2010**, *9* (3), 193–204.
- (39) Søndergaard, T.; Bozhevolnyi, S. I. *Opt. Express* **2007**, *15*, 4198–4204.
- (40) Temnov, V. V. *Nat. Photonics* **2012**, *6*, 728–736.
- (41) Zhang, J.; Zhang, L.; Xu, W. J. *J. Phys. D: Appl. Phys.* **2012**, *45* (11), 113001–113019.
- (42) Raether, H. *Springer Tracts Mod. Phys.* **1988**, *111*, 1–133.
- (43) Xu, Y. F.; Rao, H. S.; Chen, B. X.; Lin, Y.; Chen, H. Y.; Kuang, D. B.; Su, C. Y. *Adv. Sci.* **2015**, *2* (7), 1500049.
- (44) Kalachyova, Y.; Mares, D.; Jerabek, V.; Zaruba, K.; Ulbrich, P.; Lapcak, L.; Svorcik, V.; Lyutakov, O. J. *J. Phys. Chem. C* **2016**, *120*, 10569–10577.
- (45) Zhou, H.; Qu, Y.; Zeid, T.; Duan, X. *Energy Environ. Sci.* **2012**, *5* (5), 6732–6743.
- (46) Sivula, K.; Le Formal, F.; Grätzel, M. *ChemSusChem* **2011**, *4* (4), 432–449.
- (47) Ling, Y.; Wang, G.; Wheeler, D. A.; Zhang, J. Z.; Li, Y. *Nano Lett.* **2011**, *11* (5), 2119–2125.
- (48) Turner, J. E.; Hendewerk, M.; Parmeter, J.; Neiman, D.; Somorjai, G. A. *J. Electrochem. Soc.* **1984**, *131* (8), 1777–1783.
- (49) Hsu, C.-M.; Connor, S. T.; Tang, M. X.; Cui, Y. *Appl. Phys. Lett.* **2008**, *93* (13), 133109.
- (50) Li, Y.; Zhang, J.; Zhu, S.; Dong, H.; Jia, F.; Wang, Z.; Tang, Y.; Zhang, L.; Zhang, S.; Yang, B. *Langmuir* **2010**, *26* (12), 9842–9847.
- (51) Barnes, W. L.; Murray, W. A.; Dintinger, J.; Devaux, E.; Ebbesen, T. W. *Phys. Rev. Lett.* **2004**, *92* (10), 107401.
- (52) Cushing, S. K.; Hornak, L. A.; Lankford, J.; Liu, Y.; Wu, N. *Appl. Phys. A: Mater. Sci. Process.* **2011**, *103* (4), 955–958.
- (53) Li, M.; Cushing, S. K.; Zhang, J.; Lankford, J.; Aguilar, Z. P.; Ma, D.; Wu, N. *Nanotechnology* **2012**, *23* (11), 115501.
- (54) Qasem, N. A. A.; Ben-Mansour, R. *Appl. Energy* **2018**, *230*, 1093–1107.
- (55) Jeppesen, C.; Mortensen, N. A.; Kristensen, A. *Appl. Phys. Lett.* **2010**, *97* (26), 263103.
- (56) Guo, B.; Tian, L.; Xie, W.; Batool, A.; Xie, G.; Xiang, Q.; Jan, S. U.; Boddula, R.; Gong, J. R. *Nano Lett.* **2018**, *18*, 5954–5960.
- (57) Chien, F. C.; Chen, S. J. *Opt. Lett.* **2006**, *31* (2), 187–189.
- (58) Spinelli, P.; Hebbink, M.; de Waele, R.; Black, L.; Lenzmann, F.; Polman, A. *Nano Lett.* **2011**, *11* (4), 1760–1765.
- (59) Catchpole, K. R.; Polman, A. *Opt. Express* **2008**, *16*, 21793–21800.
- (60) Le Formal, F.; Grätzel, M.; Sivula, K. *Adv. Funct. Mater.* **2010**, *20* (7), 1099–1107.
- (61) Le Formal, F.; Tétreault, N.; Cornuz, M.; Moehl, T.; Grätzel, M.; Sivula, K. *Chem. Sci.* **2011**, *2* (4), 737–743.
- (62) Thimsen, E.; Le Formal, F.; Grätzel, M.; Warren, S. C. *Nano Lett.* **2011**, *11* (1), 35–43.